Received: 1 September 2021 | Revised: 18 October 2021 | Accepted: 22 October 2021

DOI: 10.1002/rra.3905

RESEARCH ARTICLE

WILEY

Physical modelling of pipe culverts to assist upstream fish passage

Zhenglong Li | Jason Harley | Hubert Chanson

School of Civil Engineering, The University of Queensland, Brisbane, QLD, Australia

Correspondence
Hubert Chanson, School of Civil Engineering, The University of Queensland, Brisbane, QLD 4072, Australia.
Email: h.chanson@uq.edu.au

Funding information
University of Queensland, School of Civil Engineering

Abstract

Road crossings and culverts may adversely impact the stream network connectivity and fish habitats of the catchment. Research into the passage of small-body-mass fish in pipe culverts has been relatively limited, compared to the literature for box culverts. For small-bodied and juvenile fish species, the excessive barrel velocities are often a major hindrance, because of their weak swimming capabilities. In the present study, some physical testing of low-velocity-zones was undertaken in standard pipe culvert. The physical modelling was conducted under controlled flow conditions to test comparatively three designs, aiming to minimise the change in energy losses and to maximise low-velocity zones and secondary circulation conducive to small-body-mass fish passage. In the whole pipe culvert experiment (Model 1), both baffle and longitudinal rail boundary treatments provided low-velocity zones. The baffles however induced a strongly turbulent flow, associated with substantially larger energy dissipation than the reference smooth boundary pipe culvert. The longitudinal rail boundary treatment produced energy losses comparable to the smooth boundary reference configuration. Both boundary treatments were tested comparatively at near-full-scale (Model 2) to quantify the low-velocity-zone (LVZ) characteristics. The small longitudinal rail (0.06 m $\times$ 0.02 m), installed at 30° from the centreline, induced some flow asymmetry, as well as some low-velocity-zones on both sides of the rail. Some strong secondary motion was further observed as the combined effect of the flow asymmetry and singularities of the rail corners. The secondary motion structure was markedly different, and the distributions of the normal turbulent stresses ($v_z'^2 - v_y'^2$) showed key differences between the two boundary treatments, with the sharp corners of the rail contributing to the generation of secondary motion and in turn slow-velocity regions facilitating the upstream passage of small-body-mass fish species and juveniles of larger fish.

KEYWORDS
fish passage, longitudinal rail, low-velocity zones, physical modelling, pipe culverts

1 | INTRODUCTION

Road crossings and culverts may adversely impact the stream network connectivity and fish habitats of the catchment (Warren Jr. & Pardew, 1998). A culvert is a narrow-covered channel designed to pass drainage flows and streams beneath a roadway (Figure 1). Their traversability by aquatic life is closely linked to the target species distributions and stream habitat quality (Januchowski-Hartley, Diebel, Doran, & McIntyre, 2014). For completeness, culverts can also assist the passage of small animals, thus reducing their road kills (Dodd Jr,

FIGURE 1 Pipe culverts in Australia. (a) Pipe culvert outlet below Market Street off Witton Creek (Indooroopilly QLD) on 6 February 2020 after more than 60–65 mm of rain in catchment in the last 8 hr. (b) Multicell pipe culvert beneath Karrabin-Rosewood Road, Walloon (QLD)—Note the lower (left) cells equipped with baffles for fish passage—Inset: details of baffles [Color figure can be viewed at wileyonlinelibrary.com]

Barichivich, & Smith, 2004; Goosem, 2002). In terms of fish passage for a given targeted species, some parameters relevant to traversability include the culvert type, the barrel dimensions, cross-sectional shape and invert slope, as well as the water discharge and fluid dynamics properties in the culvert structure (Larinier, 2002; Olsen & Tullis, 2013). For small-bodied and juvenile fish species, the excessive barrel velocities are often a major hinderance, because small-body-mass fish tend to have weak swimming capabilities (Hurst, Kay, Ryan, & Brown, 2007; Pavlov, Lupandin, & Skorobogatov, 1994; Tudorache, Viaene, Blust, Vereecken, & De Boeck, 2008), notwithstanding that swimming performance data can exhibit substantial variability in natural populations (Jones & Hale, 2020). In laboratory, the testing protocol and equipment may impact the data outcomes (Katopodis & Gervais, 2016; Kern, Cramp, Gordos, Watson, & Franklin, 2018), leading to "*inconsistent metrics*" (Kemp, 2012). While some studies suggested that the swimming performances might decrease with increased turbulence (Pavlov, Skorobogatov, & Shtaf, 1982; Shaft, Pavlov, Skorobogatov, & Barekyan, 1983), the interpretation of flow turbulence typology is critical to any boundary treatment conducive to the upstream passage, especially with small weak-swimming fish often seeking high-turbulence low-velocity zones (Chanson, 2019; Goettel, Atkinson, & Bennett, 2015). Other relevant fluid flow parameters include secondary circulation (Papanicolaou & Talebbeydokhti, 2002) and transverse velocity component, that hinder fish performances with increasing transverse current (Skorobogatov & Pavlov, 1991).

Research into the passage of small-body-mass fish in pipe culverts has been relatively limited, compared to the literature for box culverts (Chanson & Leng, 2021). On one hand, several studies stated that box culverts are more suitable for fish passage because of the greater diversity in water velocities and substrate (Briggs & Galarowicz, 2013; Doehring, Young, & McIntosh, 2011). On another side, a few field studies (Cahoon, McMahon, Solcz, Blank, & Stein, 2007; Monk & Hotchkiss, 2012; Rogers et al., 2021) showed contrasted results, with one data set showing comparable passages of Brook Trout (*Salvelinus fontinalis*) over several months in a reference site (no culvert), in a box culvert and a pipe culvert of comparable size, all sites bring located in the same water system (Rogers et al., 2021).

With pipe culverts, some computational studies tested various shapes of baffles (Feurich, Boubee, & Olsen, 2012; Khodier & Tullis, 2018). Several physical studies indicated that large roughness elements, corrugations and baffles may effectively assist the upstream passage of fish (Gigleux & de Billy, 2013; Macdonald & Davies, 2007; Olsen & Tullis, 2013; Santos et al., 2021). A few biological studies under controlled conditions at full-scale showed that small to medium-size fish tended to follow paths along low-velocity zones (LVZs) (Goerig, Bergeron, & Castro-Santos, 2017; Pearson et al., 2005), as previously reported in box culverts (Blank, 2008; Cabonce, Fernando, Wang, & Chanson, 2019; Cabonce, Wang, & Chanson, 2018; Jensen, 2014; Wang, Chanson, Kern, & Franklin, 2016).

The present investigation was inspired by the needs to facilitate the upstream passage of small-bodied and juvenile native fish species,

common to eastern Australia, in pipe culverts, but the present results may apply to other weak-swimming species. For these fish species, the characteristic swimming speed is often less than 0.6 m/s (Humphries & Walker, 2013; Hurst et al., 2007) and high water velocities in the barrel constitute a major obstacle to their upstream traversability. In the present study, the physical testing of several configurations was undertaken in standard pipe culverts. The physical modelling was conducted under controlled flow conditions to comparatively test three designs, aiming to minimise the change in energy losses and to maximise low-velocity zones and secondary circulation conducive to small-body mass fish passage. The paper finally focused on a relatively simple solution, that is, a longitudinal rail, which could be used to retrofit existing pipe culverts and for new designs.

2 | PHYSICAL FACILITIES AND EXPERIMENTAL TESTING

2.1 | Experimental facility and instrumentation

The physical experiments were conducted in the AEB Hydraulics Laboratory at the University of Queensland. Two different facilities were used (Table 1, Figures 2 and 3). A complete culvert model (Model 1) was used to simulate a single- pipe culvert, installed in a 2.5 m long 1 m wide PVC and perspex flume (Figure 2). The culvert inlet and outlet were identical, that is, 0.325 m long with 45° wingwalls. The barrel was 0.50 m long with an internal diameter $D = 0.095$ m. The flume was fed by a constant head tank and the tailwater depth was controlled by a downstream overflow gate. The second facility (Model 2) was a near-full-scale pipe culvert, placed in a 15 m long 0.5 m wide horizontal flume, ending with an overfall. A semi-circular section ($D = 0.50$ m) was installed between $x = 1.17$ m and 14.42 m, where x is the longitudinal distance from the upstream end of the flume (Figure 3).

The water discharge was measured with an orifice and a Venturi meter installed in the supply line of the Models 1 and 2 respectively. Both devices were designed based upon British Standard (1943) and calibrated in-situ. The water depths were measured using rail mounted pointer gauges. In the Model 2, velocity measurements were performed with a Prandtl-Pitot tube Dwyer™ 166 Series (Ø = 3.18 mm), a roving Preston tube (RPT) type C1.6 (r) (Ø = 1.43 mm), an acoustic Doppler velocimeter (ADV) Nortek™ Vectrino+ equipped with a side-looking head, and an acoustic Doppler velocimeter (Profiler) Nortek™ Vectrino II equipped with a side-looking head. The ADV signal was sampled at 200 Hz for 400 s at each sampling location, and the Profiler signal was sampled at 100 Hz for 540 s. The vertical position of the velocimeters were recorded with a HAFCO® digital scale unit with an accuracy of 0.05 mm. The

TABLE 1 Experimental flow conditions—comparison between present and previous related studies

Reference	S_o	D (m)	Q (m^3/s)	Configuration	Instrumentation
Present study					
Model 1	0	0.095	0.001–0.009	Smooth pipe Baffles: $L_b = 0.09$ m, $h_b = 0.010$ & 0.020 m (0.008 m thickness), $\theta = 0, 10, 20, 30, 45°$ Longitudinal rail: $h_b = 0.005, 0.010, 0.020$ m, $\theta = 0, 10, 20, 30, 45°$	Pointer gauge
Model 2	0	0.50	0.025–0.075	Smooth pipe	Pointer gauge, Prandt-Pitot tube, RPT, ADV
			0.055–0.075	Longitudinal rail: $h_b = 0.060$ m, $\theta = 30°$	
Rajaratnam and Katopodis (1990)	0 to 0.05	0.305	0.001 to 0.070	Baffles: $L_b = 0.183$ & 0.366 m, $h_b = 0.0305$ & 0.046 m, $\theta = 0°$	Pointer gauge, Prandt-Pitot tube
Olsen and Tullis (2013)[a]	0 to 0.035	0.573	0.018 to 0.131	Baffles: $L_b = 0.515$ m, $h_b = 0.086$ m, $\theta = 0, 10°$	Pointer gauge
Khodier and Tullis (2014)[b]	0.03 to 0.06	0.573	0.0283, 0.0565, 0.085	Baffles: $L_b = 0.515$ m, $h_b = 0.086$ m, $\theta = 0°$	Video camera
Khodier and Tullis (2018)	0.005 to 0.06	0.570	0.0283, 0.0565, 0.085	Baffles: $L_b = 0.514$ m, $h_b = 0.086$ m, $\theta = 0°$	Pointer gauge, PIV
Chanson (2020)	0	0.50	0.055	Longitudinal rail: $h_b = 0.030$ m, $\theta = 30°$	Pointer gauge, Prandt-Pitot tube, ADV
Tonkin et al. (2012)[c]	0.18	0.35	0.0009 to 0.001	Mussel spat rope: Ø = 14 mm (core)	Pointer gauge, dye tracer

Note: ADV, acoustic Doppler velocimetry; D, internal pipe diameter; h_b, baffle/rail height; L_b, longitudinal baffle spacing; PIV: particle image velocimetry; Q, water discharge; S_o, bed slope; θ, tilt of baffle/rail.

[a]Experiments with wild brown trout (*Salmo trutta morpha fario* and *S. trutta morpha lacustris*).

[b]Experiments with wild brown trout (*Salmo trutta*).

[c]Experiments with redfin bully (*Gobiomorphus huttoni*).

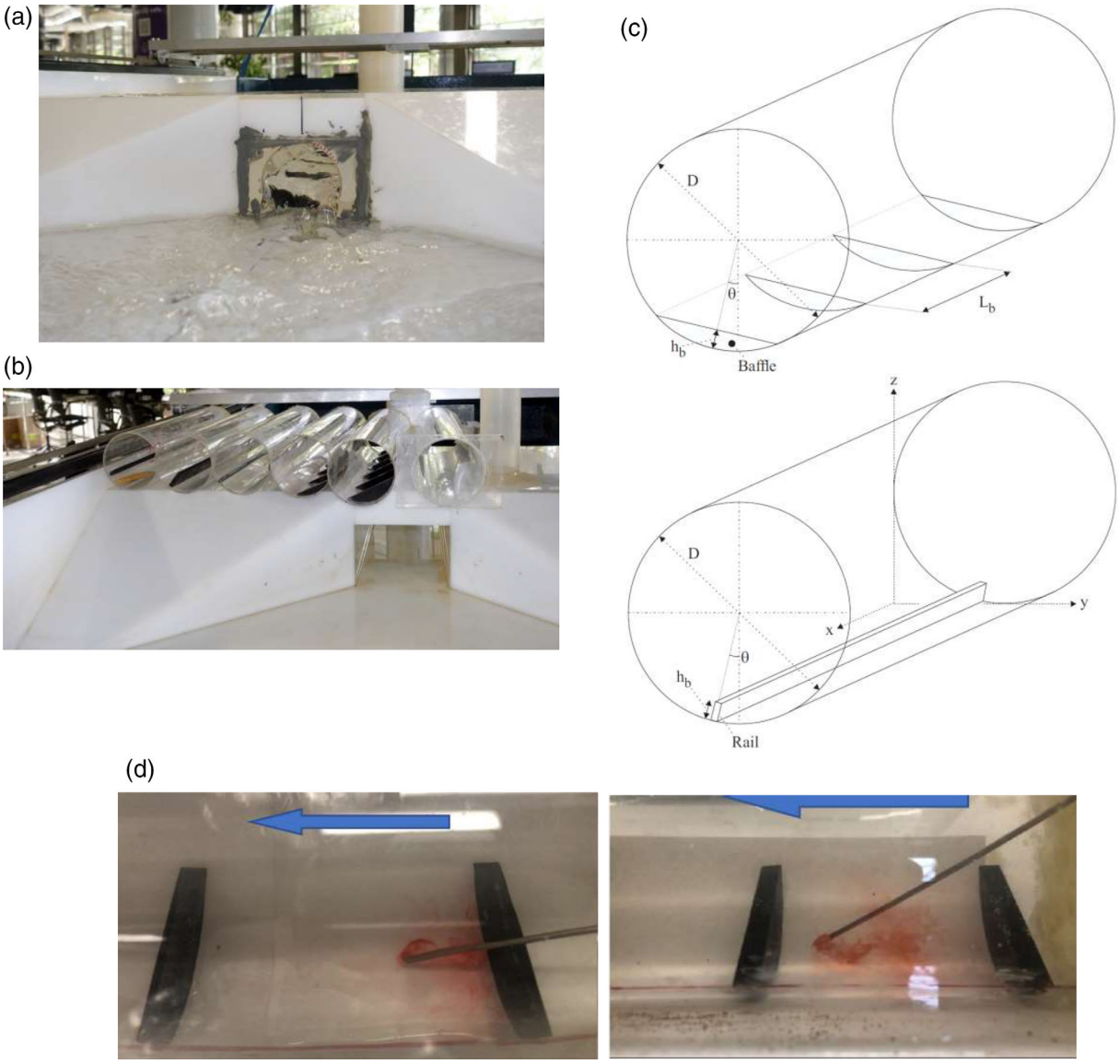

FIGURE 2 Pipe culvert model and testing configurations. (a) Pipe culvert model outlet with baffles ($h_b = 0.020$ m, $L_b = 0.09$ m, $\theta = 10°$) operating with free-surface flow for $Q = 0.004$ m^3/s. (b) Barrel designs with longitudinal ribs (0.020 m, 0.095 m, 0.010 m), baffles (0.010 m, 0.020 m) and smooth configuration from left to right. (c) Definition sketch of the baffled and longitudinal rail pipe culvert configurations. (d) Photographs of low-velocity zones and recirculation regions in the baffled pipe culvert barrel highlighted by dye injection—Flow direction from right to left. (d1) Dye injection in the middle of the baffled barrel ($h_b = 0.010$ m, $L_b = 0.09$ m, $\theta = 10°$) for $Q = 0.001$ m^3/s and $d_{tw} = 0.06$ m—Blue arrow shows the main flow direction. (d2) Dye injection at the upstream end of the baffled barrel ($h_b = 0.020$ m, $L_b = 0.09$ m, $\theta = 20°$) for $Q = 0.002$ m^3/s and $d_{tw} = 0.09$ m [Color figure can be viewed at wileyonlinelibrary.com]

ADV data processing included the removal of communication errors, of average signal to noise ratio data less than 5 dB and of average correlation values less than 60%, while the phase-space thresholding technique was applied (Goring & Nikora, 2002; Wahl, 2003). While some ADV signal scattering was induced by the curved invert surface (Chanson, 2020; Garner, 2011), the percentage of good samples was typically greater than 90% at all sampling locations during the current study.

In both facilities, flow visualisations were undertaken with dye injection and wool strings, complemented by digital photographic and movie recordings (Figure 3 and Appendix I).

2.2 | Boundary treatments

In the whole culvert model (Model 1), three boundary treatments were tested: smooth pipe, baffles, and a longitudinal rail (Table 1 and Figure 2b). The reference configuration was a smooth pipe barrel. The baffles were installed 0.95 × D apart ($L_b = 90$ mm), the baffle height was 0.105 × D ($h_b = 10$ mm) or 0.21 × D ($h_b = 20$ mm), and the tilt angle was $\theta = 0$, 10, 20, 30 or 45° (Figure 2c). The first baffle was installed 0.030 m from the upstream end of the barrel. The ratio L_b/h_b was 9 and 4.5 for the small and large baffles respectively. For comparison, Olsen and Tullis (2013) used a similar baffled culvert

FIGURE 3 Full-scale pipe culvert barrel channel with 0.060 m × 0.020 m rail installed at $\theta = 30°$. Left: Looking upstream for $Q = 0.065$ m^3/s, with the longitudinal rail seen on the left of the photograph (Arrow). Middle: Dye plume advected along the lower (left) side of the rail for $Q = 0.075$ m^3/s. Right: Dye plume advected along the upper (right) side of the rail for $Q = 0.075$ m^3/s. The dye was injected at $x = 2.0$ m and the photograph were taken at $x = 7.15$ m looking upstream [Color figure can be viewed at wileyonlinelibrary.com]

configuration with $h_b/D = 0.15$, $L_b/h_b = 6$ and $\theta = 0$ or 10° (Table 1). The third configuration, a longitudinal rail, was motivated by a recent study showing the positive impact of longitudinal mussel spat rope on upstream passage of small fish (Tonkin, Wright, & David, 2012). The rail was installed for the full length of the barrel at a tilt angle $\theta = 0$. 10, 20, 30 or 45°, with 45° bezel ends. Three rail sizes were tested: $h_b = 0.005$, 0.010, and 0.020 m.

In the near-full-size barrel channel (Model 2), two boundary treatments were investigated: a smooth pipe and a longitudinal rail (Table 1 and Figure 3). In the latter configuration, a longitudinal rail was installed at $\theta = 30°$ from the centreline vertical. The rail was 0.020 m wide, 0.060 m high ($h_b = 0.060$ m), and 13.25 m long. The rail configuration corresponded to a 6:1 upscaled version of the Model 1 configuration with $h_b = 0.010$ m.

2.3 | Experimental flow conditions

The physical investigations were performed with flow rates within 0.001 m^3/s < Q < 0.008 m^3/s in the Model 1 and tailwater depths between 0.010 m and 0.100 m for all boundary treatments. The observations focused on the flow patterns, including recirculation and low-velocity zones, and on the afflux-discharge relationship for each pipe culvert configuration. All the experiments were performed with increasing flow rates, to avoid hysteresis (Montes, 1997).

In the Model 2, the flow patterns and free-surface measurements were conducted for 0.015 m^3/s < Q < 0.075 m^3/s. The velocity measurements were performed for 0.025 m^3/s < Q < 0.075 m^3/s in the smooth pipe and 0.055 m^3/s < Q < 0.075 m^3/s in the pipe culvert barrel with longitudinal rail. For each boundary treatment, the velocity data were collected for 0.025 m < y < 0.475 m where y is the transverse distance from the right sidewall. With the longitudinal rail, a total of 14 velocity profiles were recorded for each flow rate, with a minimum of 25 data points per profile, except in shallow waters at the outer edges.

3 | PIPE CULVERT HYDRAULICS

3.1 | Flow patterns

In the smooth pipe culvert, that is, reference boundary treatment, the flow in the inlet and barrel entrance was smooth and waveless, without any sign of flow separation. The flow-velocity increased in the barrel as a result of the reduction in cross-sectional area. The culvert outlet flow was very turbulent for all investigated conditions. At low tailwater levels, the outlet flow was supercritical and a three-dimensional free hydraulic jump took place downstream of the outlet. At high tailwater, a high-speed jet discharged out of the downstream end of the barrel, with strong recirculation and large-scale vortices in the outlet and downstream channel (Figure 2a and Movie M1). The Movie M1 (Appendix I) shows the outlet operation of a multi-pipe culvert with the barrel operating half-full. In the movie, strong turbulence, waves and recirculation can be seen in the outlet. Figure 4a presents a typical relationship between the upstream flow depth d_1 and tailwater depth d_{tw} for a given flow rate. At low tailwater levels, the pipe culvert operated with inlet control and the tailwater level had no impact on the upstream water levels. Once outlet control was reached, the upstream depth increased with increasing tailwater depth (Figure 4a).

At low discharges, the flow in pipe culverts was a free-surface flow for all boundary treatments and investigated tailwater conditions $0.105 < d_{tw}/D < 1.05$. With increasing discharges, the barrel flowed full at large tailwater depths. The observations of the transition from free-surface flow to full barrel are reported in Figure 4b. The results in terms of transition flow conditions were basically identical for the

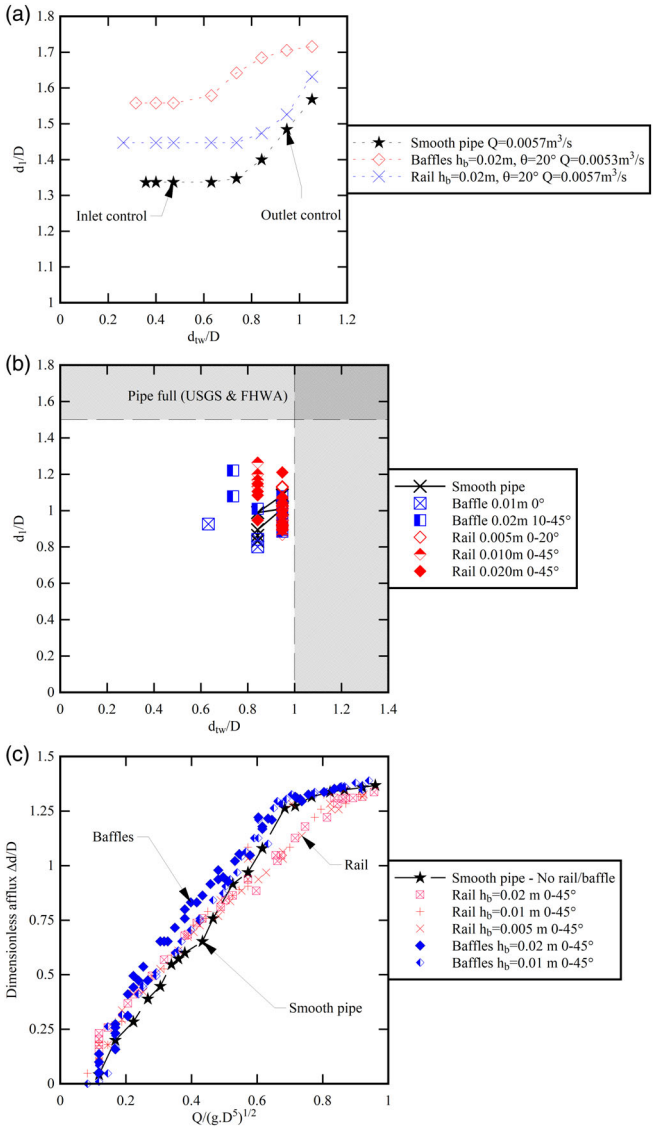

FIGURE 4 Hydraulic of pipe culvert model ($D = 0.095$ m, $S_o = 0$). (a) Dimensionless relationship between the upstream depth d_1/D and tailwater depth d_{tw}/D for smooth pipe culvert, baffled barrel culvert ($h_b = 0.020$ m, $L_b = 0.09$ m, $\theta = 20°$) and longitudinal rail culvert ($h_b = 0.020$ m, $\theta = 20°$) for $Q/(g \times D^5)^{1/2} \sim 0.065$. (b) Dimensionless relationship between the upstream depth d_1/D and tailwater depth d_{tw}/D at the end of free-surface barrel flow. Comparison between smooth pipe culvert, baffled barrel culvert and longitudinal rail culvert data with USGS and FHWA guidelines for barrel flowing full (shaded areas). (c) Dimensionless relationship between afflux $\Delta d/D$ and discharge $Q/(g \times D^5)^{1/2}$ for smooth pipe culvert (Black stars and thick dashed line) and pipe culvert equipped with baffles (Blue diamond symbols) and with longitudinal rail (Red cross symbols). Tailwater condition: $d_{tw}/D = 0.40$ [Color figure can be viewed at wileyonlinelibrary.com]

smooth pipe and longitudinal rail configurations, with a slightly earlier transition with the baffles. Although the tilt of appurtenance had no effect on the onset of transition, the size of baffles had some slight impact (Figure 4b). The present data are further compared with the range of conditions reported by the USGS and FHWA (Bodhaine, 1968; Chin, 2013), showing some agreement (Figure 4b) although the present data were slightly outside of these guidelines (i.e., shaded areas).

With the baffle boundary treatment, the observations indicated a slower motion in the barrel compared to the smooth pipe for the same discharge and tailwater conditions. The flow appeared more turbulent as evidenced by free-surface disturbances and waves in the barrel. Dye injections showed some flow recirculation occurring between the baffles, irrespective of the tilt angle (Figure 2d). No other obvious recirculation region was observed within the pipe barrel. Figure 2d presents photographs of the recirculation motion in the cavity between baffles. The Movie M2 (Appendix I) shows the recirculation between two baffles, visualised with dye injection. The low-velocity zone and recirculation region extended over the full cavity length between adjacent baffles, and the current observations were consistent with the PIV data of Khodier and Tullis (2018).

With the longitudinal rail, both dye injection and the use of woollen strings assisted the visualisation of flow patterns. Unlike the baffled culvert design, there was no obvious recirculation nor strong free-surface turbulence in the barrel. Visual observations suggested that the rail induced elongated longitudinal eddies on both sides of the rail. With some tilt (θ >0), the eddies tended to be larger above the rail than below. As the discharge increased, larger eddies were observed on both sides of the rail.

3.2 | Afflux-discharge relationship

The relationship between discharge and afflux was investigated for all boundary treatments including the reference smooth pipe culvert, for the flow conditions listed in Table 1. The afflux is defined as the rise in upstream water level caused by the culvert: $\Delta d = d_1 - d_{tw}$ with d_1 the upstream water depth and d_{tw} the tailwater depth. The afflux data are presented in Figure 4c, with the black star symbols for the reference boundary treatment. Overall, the smooth pipe culvert yielded the smallest afflux for $Q/(g \times D^5)^{0.5} < 0.5$ and all tailwater levels, which corresponded to free-surface inlet flow conditions. For $Q/(g \times D^5)^{0.5} > 0.5$, that is, submerged inlet, the smallest afflux was achieved with the longitudinal rail configurations, irrespective of the rail dimensions, possibly because of the flow streamlining induced by the rail. For $Q/(g \times D^5)^{0.5} > 0.85$, the embankment was overtopped for all boundary treatments and all the data collapsed (Figure 4C).

Overall, the largest afflux was systematically observed with the baffle designs for all flow conditions, with a larger afflux for the largest baffles ($h_b/D = 0.21$), linked to the increased roughness, in line with previous data (Khodier & Tullis, 2014; Olsen & Tullis, 2013; Rajaratnam & Katopodis, 1990). Compared to the smooth pipe, the baffled pipe culvert data presented a dimensionless increase in afflux $\Delta d/D$ of 0.2–0.25: that is, 25–50% increase in afflux depending upon the dimensionless discharge (Figure 4c). The results demonstrated a higher discharge capacity in pipe culverts equipped with longitudinal rail than in baffled pipe culverts. While the comparison between baffle and longitudinal rail was expected, the present findings showed

further an even greater discharge capacity at large discharges compared to the reference smooth pipe boundary treatment (Figure 4c).

With both baffle and rail boundary treatments, the flow visualisations based upon dye injection highlighted low-velocity zones and recirculation regions which were considered as potential zones to assist upstream fish passage. But the energy losses were greater with the baffles. Although the longitudinal rail induced elongated low-velocity zones on both sides of the rail, their size could not be visualised in Model 1. Further experiments were conducted in near-full-scale pipe culvert barrel model (Model 2) to quantify the low-velocity-zone properties.

4 | PIPE CULVERT BARREL HYDRODYNAMICS

4.1 | Presentation

In the near-full-scale pipe culvert barrel (Model 2), detailed free-surface and velocity measurements were conducted in the middle of the barrel at $x = 7.15$ m. Typical results are presented in terms of the time-averaged longitudinal velocity in Figure 5. Owing to the presence of the free-surface and to the boundary friction along the wetted perimeter, the velocities in the smooth boundary pipe were not uniformly distributed, with slower flow next to the invert (Figure 5a). Further, dye injection showed the existence of large elongated streamwise structures in the mainstream, likely initiated by secondary currents (see below). Complicated upwelling and downwelling longitudinal streaks were seen, similar to those reported by Imamoto and Ishigaki (1986) and Tamburrino and Gulliver (2007).

In presence of the longitudinal rail, low-velocity zones were evidenced on both sides of the rail (Figures 3 and 5b, Movie M3). The Movie M3 (Appendix I) shows the visualisation of low-velocity zone along the rail. The dye was injected in the inner corner below the rail. The dye cloud maintained its coherence for the full length of the rail (i.e., 13.25 m). The longitudinal rail induced some flow asymmetry, similar to earlier findings in circular and rectangular channels (Chanson, 2020; Sanchez, Leng, Von Brandis-Martini, & Chanson, 2020) (Figure 5b).

The longitudinal velocity maps were integrated to check for continuity (i.e., conservation of mass):

$$< Q > = \int_A V_x \times dy \times dz \quad (1)$$

The results were in close agreement with the discharge measurements using the Venturi meter within less than 4%. The non-uniformity of the velocity distributions was characterised by the kinetic energy and momentum correction coefficients, α and β respectively, used in one-dimensional hydraulic modelling (Henderson, 1966; Montes, 1998). The present data are shown in Table II-1 and Figure II-1 (Appendix II), with α and β being defined as:

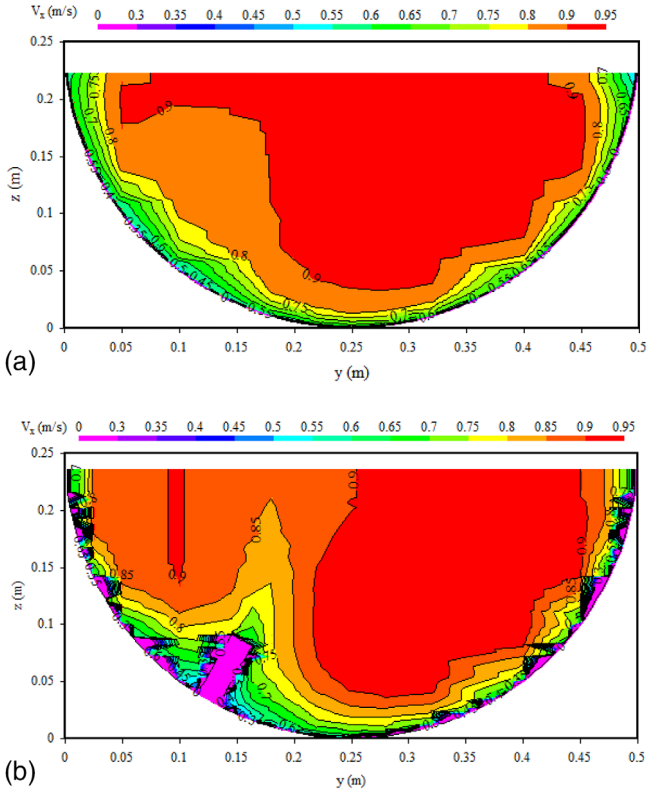

FIGURE 5 Contour maps of constant time-averaged longitudinal velocity V_x in the near-full-scale pipe culvert barrel (Model 2) with smooth boundary and with longitudinal rail—$Q = 0.075$ m^3/s, $x = 7.15$ m, $y = 0.25$ m at the centreline and $y = 0$ at right glass sidewall, velocity scale in m/s, Prandtl-Pitot tube and roving Preston tube data. (a) Contour plot in the smooth pipe culvert barrel, $d = 0.223$ m. (b) Contour plot in the pipe culvert barrel with longitudinal rail, $d = 0.235$ m [Color figure can be viewed at wileyonlinelibrary.com]

$$\alpha = \frac{\int_A {V_x}^3 \times dy \times dz}{{V_{mean}}^3 \times A} \quad (2)$$

$$\beta = \frac{\int_A {V_x}^2 \times dy \times dz}{{V_{mean}}^2 \times A} \quad (3)$$

Although the overall data showed some scatter (Appendix II), the present results suggested a limited impact of the longitudinal rail on the velocity correction coefficients.

The turbulent velocity fluctuations were recorded with the ADV velocimeters. Some typical velocity fluctuation maps are presented in Figure 6 for the smooth pipe culvert (Figure 6, left) and the configuration with the longitudinal rail (Figure 6, right). In Figure 6, each contour map included more than 150 measurement points, with a greater number of readings in the longitudinal rail configuration. The largest longitudinal velocity fluctuations were recorded next to the invert in the smooth pipe culvert, as well as next to the rib in the configuration with the longitudinal rail (Figure 6a). In terms of the transverse and vertical velocity fluctuations, large fluctuations were recorded

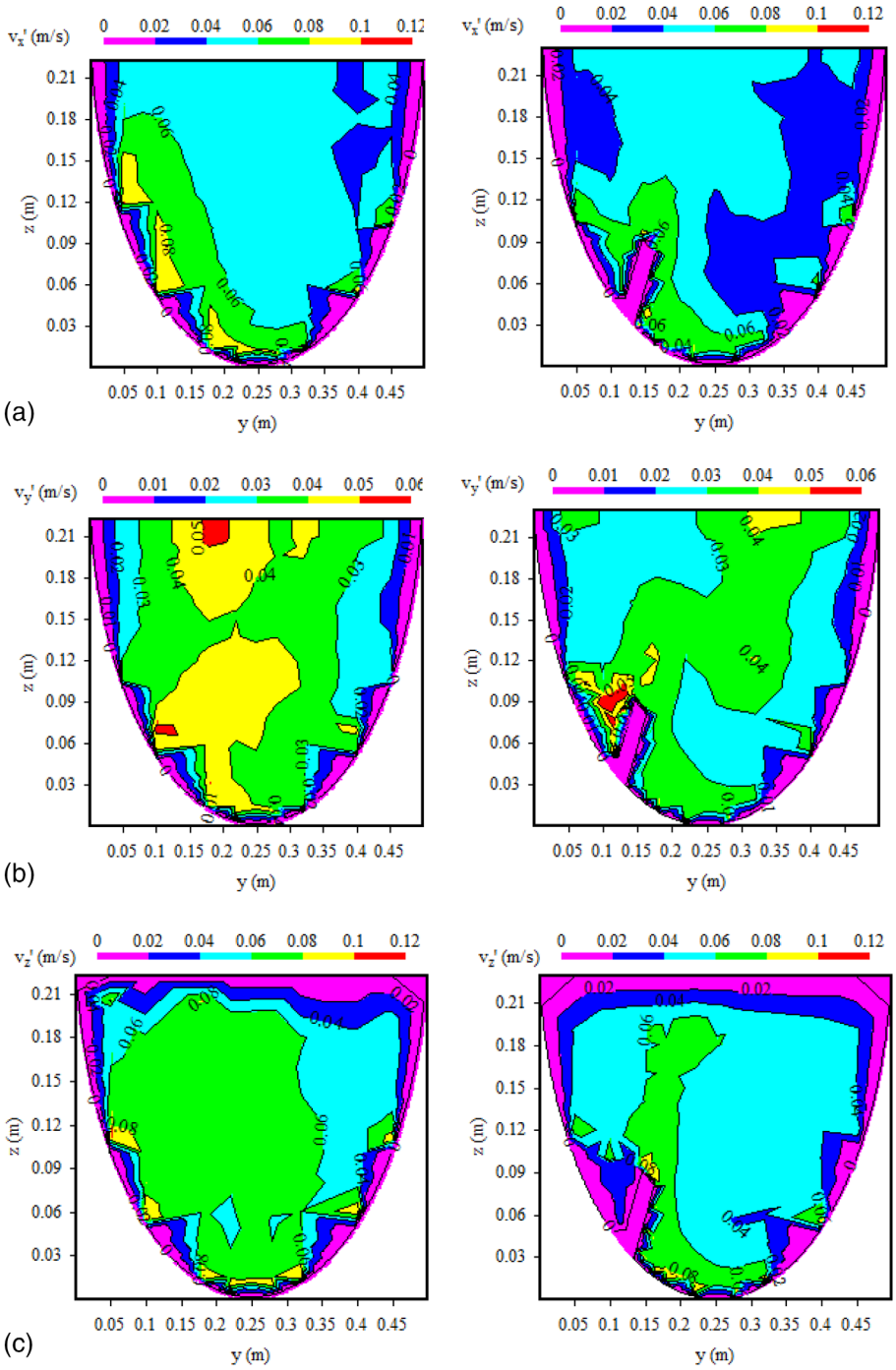

FIGURE 6 Contour maps of constant velocity fluctuations in the near-full-scale pipe culvert barrel (Model 2) with smooth boundary (left) and with longitudinal rail (right)—$Q = 0.075$ m^3/s, $x = 7.15$ m, $d = 0.223$ m (smooth boundary) and 0.230 m (longitudinal rail), $y = 0.25$ m at the centreline and $y = 0$ at right glass sidewall, velocity scale in m/s, ADV Vectrino+ (smooth boundary & rail) and Vectrino II (rail only) data [Color figure can be viewed at wileyonlinelibrary.com]

throughout the entire flow cross-sections for all discharges and both boundary treatments. The large fluctuations were linked to the existence of marked secondary circulation.

4.2 | Secondary flow motion

Secondary circulation occurs in open channel flows, irrespective of the cross-section shape and boundary treatment, because of turbulence anisotropy (Perkins, 1970; Prandtl, 1926; Prandtl, 1952). Secondary currents are directed at right angle with the longitudinal flow direction, that is, in the *y*-*z* plane, and they redistribute the momentum across the channel cross-section (Naot & Rodi, 1982).

For the investigated flow conditions (d/D <0.5), the secondary circulation in the smooth boundary pipe culvert presented a primary large circulation about the channel centreline (Figure 7a). Some lesser circulation was seen using dye injection in the upper corners, although the proximity of the free-surface prevented the operation of the ADV velocimetry. More generally, the secondary circulation near the water surface contributed to the occurrence of the velocity dip phenomenon seen in the longitudinal velocity contour map (Figure 5a). The presence of the longitudinal rail created some

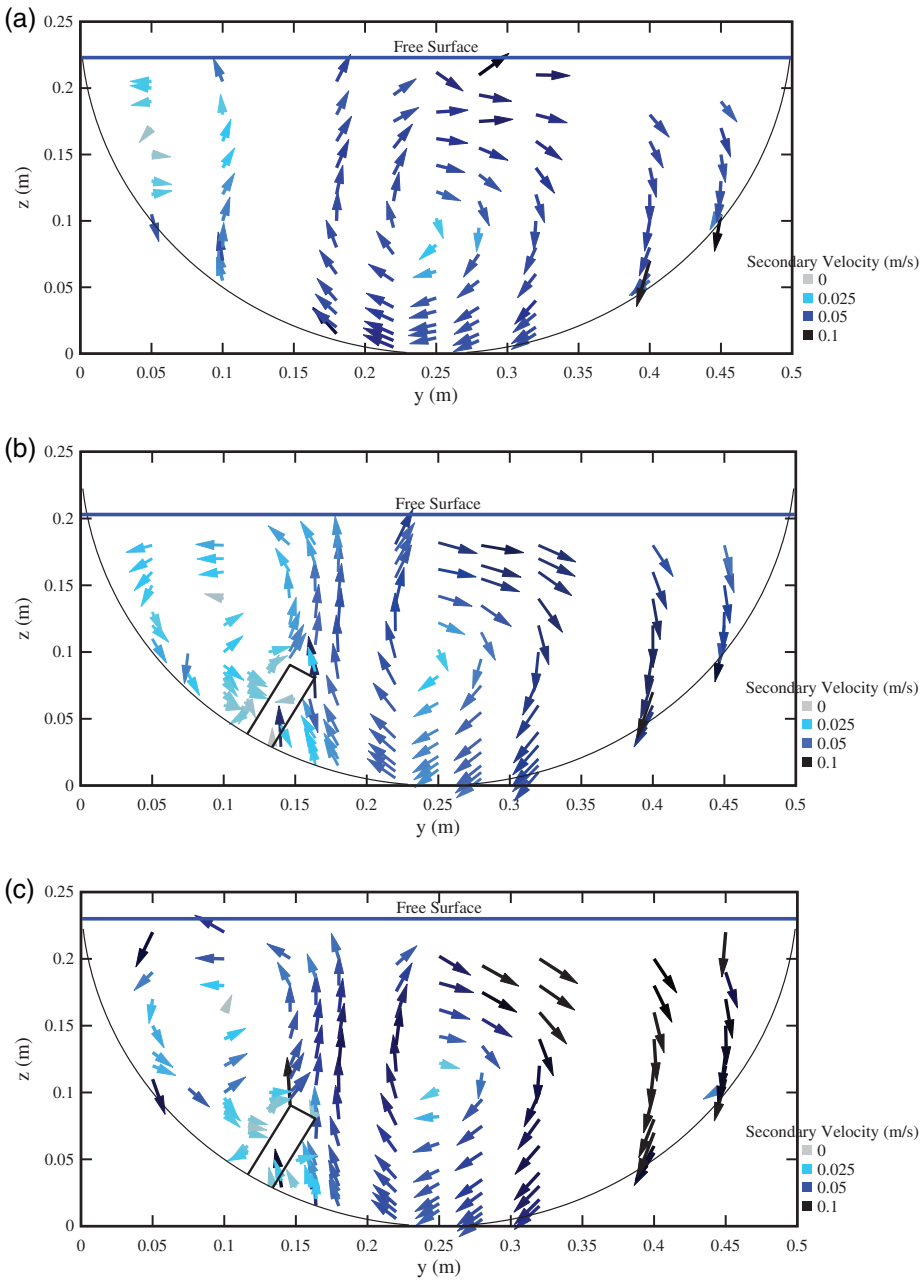

FIGURE 7 Secondary recirculation in the near-full-scale pipe culvert barrel (Model 2) with smooth boundary and with longitudinal rail—$x = 7.15$ m, $y = 0.25$ m at the centreline and $y = 0$ at right glass sidewall, secondary current velocity scale in m/s, ADV Vectrino+ and Profile Vectrino II data. (a) Smooth boundary, $Q = 0.075$ m^3/s, $d = 0.223$ m. (b) With longitudinal rail, $Q = 0.055$ m^3/s, $d = 0.203$ m. (c) With longitudinal rail, $Q = 0.075$ m^3/s, $d = 0.230$ m [Color figure can be viewed at wileyonlinelibrary.com]

asymmetrical velocity field conducive to some strong secondary circulation (Figures 3b,c). The longitudinal rail was favourable to the development of small longitudinal structures on each side of the rail, visualised with dye injection (Figure 3), as well as two large-scale vortices within the bulk of the flow (Figures 5b and 7b,c). The two large structures extended up to the water surface for $0.4 < y/D < 0.8$ for the largest secondary structure, and for $0 < y/D < 0.3$ for the smaller structure. Further, an upward secondary motion was seen above the outer edge of the rail. For the present investigations, the magnitude of the secondary current was in the order of 0.06 to $0.12 \times V_{mean}$ for both boundary treatments, with V_{mean} the bulk velocity. The secondary velocities were comparatively larger than observations in rectangular open channels (Nezu & Rodi, 1985; Tominaga, Nezu, Ezaki, & Nakagawa, 1989).

Despite its small physical size (0.06×0.02 m^2), the longitudinal rail created two outer and two inner sharp corners, that generated some transverse circulation, directed towards the corner edge because of the turbulent shear stress gradients normal to the bisector (Gessner, 1973; Liggett, Chiu, & Miao, 1965). Secondary motion may develop naturally, particularly when the difference in turbulent normal stresses ($v_z'^2 - v_y'^2$) is non zero (Gerard, 1978; Nezu & Nakagawa, 1993). The difference ($v_z'^2 - v_y'^2$) characterises the streamwise vorticity generation (Perkins, 1970; Tominaga et al., 1989), and typical results are presented in Figure 8. The comparison between Figures 8a,b is striking, because the contour map data of ($v_z'^2 - v_y'^2$) basically determined the structure of the secondary circulation. In the smooth pipe, the distributions of ($v_z'^2 - v_y'^2$) presented a similar pattern to that in rectangular channels (Tominaga et al., 1989), with

negative values towards the outer flow regions (Figure 8a). The corners of the longitudinal rail caused abrupt spatial variations in boundary conditions, inducing stable secondary motion near the inner corners on both sides of the rail, as well as larger structures on either side of bisectors from the outer corners (Figure 8b). Noteworthy, the strength of secondary circulation was closely linked to the sharpness of the outer corners (Gessner, 1973; Sanchez et al., 2020). The secondary structure pattern is sketched in Figure 8b.

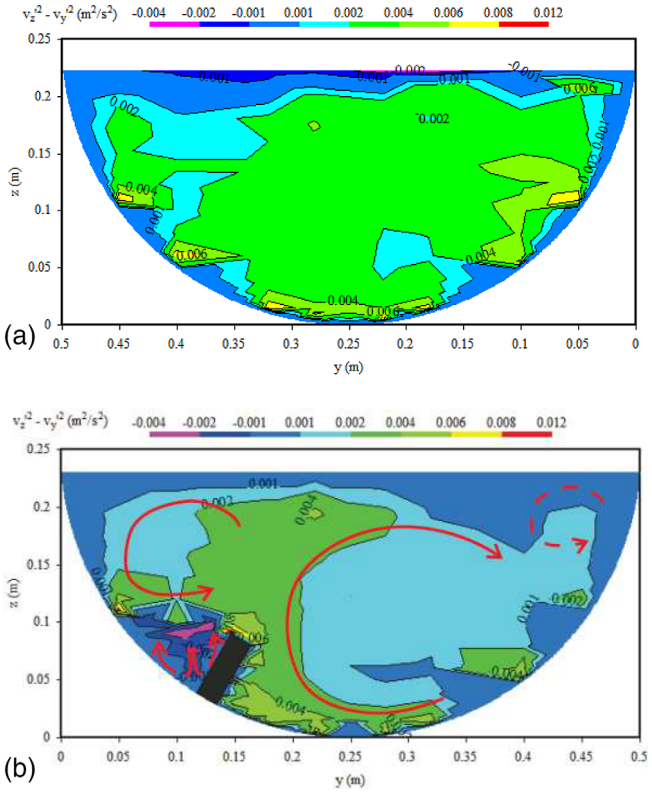

FIGURE 8 Contour maps of the difference ($v_z'^2 - v_y'^2$) in the near-full-scale pipe culvert barrel (Model 2) with smooth boundary and with longitudinal rail—$Q = 0.075$ m^3/s, $x = 7.15$ m, $y = 0.25$ m at the centreline and $y = 0$ at right glass sidewall, velocity scale in m/s, ADV Vectrino+ (smooth boundary & rail) and Vectrino II (rail only) data. (a) Smooth boundary, $d = 0.223$ m. (b) With longitudinal rail, $d = 0.230$ m—Solid red arrows indicate large secondary structures and dashed red arrows mark smaller structures [Color figure can be viewed at wileyonlinelibrary.com]

4.3 | Low-velocity zones

The longitudinal velocity data presented sharp differences between the no-slip condition ($V_x = 0$) at the invert and the maximum velocity about the channel centreline (Figure 5). The results were analysed in terms of the total area of low-velocity zone (LVZ) as well as the LVZ dimensions to ensure that they would encompass the size of the targeted fish species. Figure 9 presents the fraction of the cumulative low-velocity zone where the longitudinal velocity V_x was less than a percentage of the bulk velocity V_{mean}, that is, $V_x < V_{mean}$. In other words, the value of V_x/V_{mean} is shown in the lower axis of the graph as a percentage. In Figure 9, for a targeted fish swimming speed, a larger LVZ facilitates the upstream fish traversability. Although the size of the LVZ was comparatively smaller in pipe culverts than in box culvert, the present data compared reasonably well to earlier studies in smooth circular channels (Chanson, 2020; Sterling, 1998). The presence of the longitudinal rail ($h_b = 0.06$ m) increased substantially the LVZ area, by nearly a factor of two (Figure 9). It is believed that the LVZ's increased size was primarily generated by the secondary motion induced by the rail and its sharp corners.

The LVZs on both sides of the rail (Figures 3 and 5b) might constitute preferential swimming paths for small-bodied and juvenile fish species. Some elliptical shapes were used to characterise the physical size of these low-velocity zones (LVZs) using the software AutoCAD (Figure 10a). Only the LVZs next to the rail were considered, and ellipses with minor radius less than 0.005 m were ignored. The results are presented in Figure 10b, in terms of vertical dimensions of the ellipsoidal LVZs beside the longitudinal rail. The data for three boundary configurations were compared: smooth boundary, 0.030 m rail and

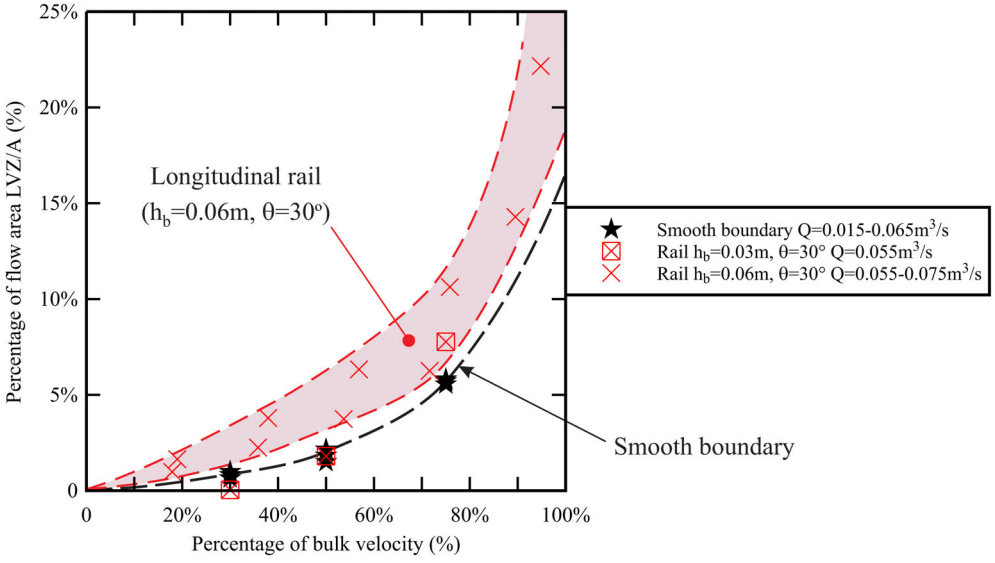

FIGURE 9 Low-velocity zone area (LVZ) relative to the flow cross-section A in the near-full-scale pipe culvert barrel (Model 2) with smooth boundary and with longitudinal rail: fractions of LVZ where $V_x = V_{mean}$ is less than a set value at $x = 7.15$ m—Comparison between present data (smooth boundary) and rail ($h_b = 0.06$ m) and data by Chanson (2020) (rail, $h_b = 0.03$ m) [Color figure can be viewed at wileyonlinelibrary.com]

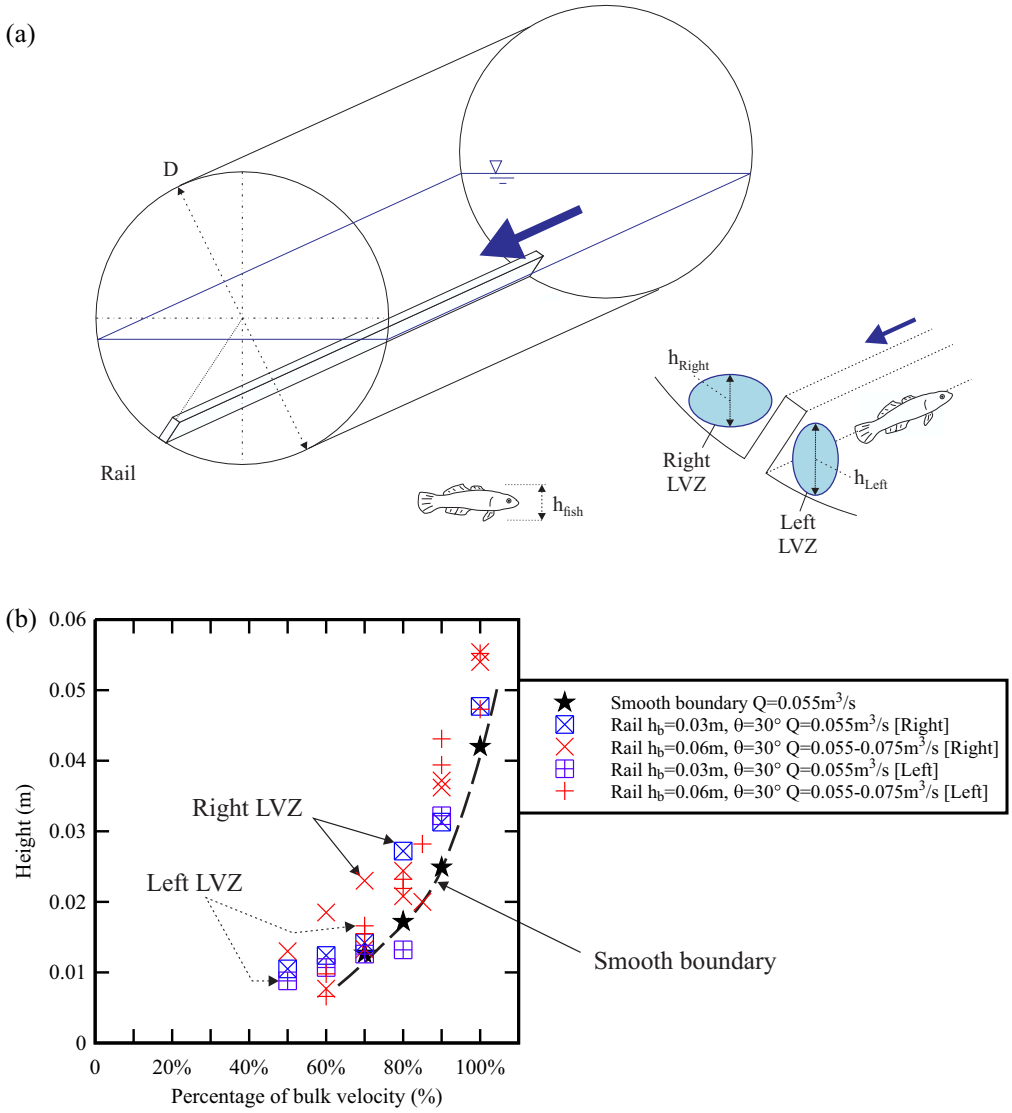

FIGURE 10 Low-velocity zone (LVZ) dimensions in the near-full-scale pipe culvert barrel (Model 2) with smooth boundary and with longitudinal rail—Data sets: Chanson (2020), Present data. (a) Definition sketch of the low-velocity zones' vertical dimension beside the longitudinal rail (b) Vertical dimensions h_{Right} and h_{Left} of the low-velocity zone with smooth boundary and with longitudinal rail—Data: Chanson (2020), Present study [Color figure can be viewed at wileyonlinelibrary.com]

0.060 m rail. The data showed a monotonic relationship between the LVZ height and the percentage of the mean flow-velocity. Furthermore, the vertical size of the right LVZ was systematically the larger than that of the left LVZ, that is, on the right of the longitudinal rail when looking downstream, for the slower flow regions with $V_x/V_{mean} < 0.7$.

Practically, let us consider some targeted fish species that would require a minimum vertical height of 0.025 m (Leng, Chanson, Gordos, & Riches, 2021). Based upon Figure 10b, the 0.025 m high LVZ would have local velocities less than 0.80 m/s for the smooth boundary pipe culvert and a water discharge $Q = 0.075$ m^3/s, when the pipe was near half full and the bulk velocity was 0.89 m/s (-Table II-1). For the same discharge, the LVZ would encompass a flow region with longitudinal velocities slower than 0.67 m/s with the 0.06 m high longitudinal rail, with a bulk velocity of 0.84 m/s (Table II-1). "Thinking like a fish" (Williams, Armstrong, Katopodis, Larinier, & Travade, 2012) (Figure 10a right), the swimming speed requirement would be 17% slower in presence of the rail, and the fish would expend 40% less power during swimming in the LVZ because the rate of work required by the fish to deliver thrust is proportional to the cube of the local water velocity (Wang & Chanson, 2018).

5 | CONCLUSION

The present study aimed to facilitate the upstream passage of small-bodied and juvenile fish species in pipe culverts. In a pipe culvert, the high water velocities in the barrel and the absence of sizeable low-velocity-zone constitute a major hindrance. Physical testing of pipe culverts was conducted under controlled flow conditions to compare three boundary treatments. These treatments aimed to minimise the change in energy losses, to maximise low-velocity zones and to generate secondary circulations conducive to small-body-mass fish passage, although the boundary treatment impact on fish behaviour was not tested. A smooth boundary pipe was used as the reference configuration. In a whole pipe culvert model, two further boundary treatments were tested: that is, baffles and longitudinal rail. The study then focused on testing a relatively simple solution, that is, a small

longitudinal rail (0.06 m × 0.02 m) in a near-full-scale pipe culvert barrel ($D = 0.5$ m).

In the whole pipe culvert experiment (Model 1), both baffle and longitudinal rail boundary treatments provided low-velocity zones: that is, with recirculation regions between each baffle and with elongated low-velocity-zones along the rail respectively. The baffles however induced a strongly turbulent flow, associated with substantially larger energy dissipation and afflux than the reference smooth boundary pipe culvert. The longitudinal rail boundary treatment produced somehow comparable energy losses than the smooth boundary reference configuration. Thus, both were tested comparatively at near-full-scale (Model 2) to quantify the low-velocity-zone (LVZ) characteristics.

In the pipe culvert barrel (Model 2), the small longitudinal rail, installed at 30° from the centreline, induced some flow asymmetry, as well as some low-velocity zones on both sides of the rail. A strong secondary motion was observed in the rail configuration, induced by the flow asymmetry and singularities of the rail corners. The secondary motion structure was markedly different, and the distributions of the normal turbulent stresses ($v_z'^2 - v_y'^2$) showed key differences between the two boundary treatments, with the sharp corners of the rail contributing to the generation of secondary motion and in turn low-velocity zones conducive to the upstream passage of small-body mass fish species and juveniles of larger fish.

Finally, the present physical experiments were performed for a range of flow conditions corresponding to less-than-design flows for a subcritical free-surface flow in the pipe culvert barrel. The proposed fish-friendly pipe culvert design with rail still needs to be verified in a field situation, and adjustments might be necessary.

ACKNOWLEDGEMENTS

The authors acknowledge the technical assistance of Jason Van Der Gevel and Stewart Matthews (The University of Queensland). They further thank the anonymous reviewers for their detailed comments. The financial support of the University of Queensland, School of Civil Engineering is acknowledged.

DATA AVAILABILITY STATEMENT

The data that support the findings of this study are available from the corresponding author upon reasonable request.

ORCID

Jason Harley https://orcid.org/0000-0003-1869-3362
Hubert Chanson https://orcid.org/0000-0002-2016-9650

REFERENCES

Blank, M. D. (2008). *Advanced studies of fish passage through culverts: 1-D and 3-D hydraulic modelling of velocity, fish energy expenditure, and a new barrier assessment method*. (Ph.D. thesis). Montana State University, Department of Civil Engineering, 231 pages.

Bodhaine, G. K. (1968). "Measurement of peak discharge at culverts by indirect methods. *Techniques of water-resources investigations of the United States Geological Survey*. Chapter A3. Denver CO: US geological survey, Department of Interior, 69 pages.

Briggs, A. S., & Galarowicz, T. L. (2013). Fish passage through culverts in Central Michigan Warmwater streams. *North American Journal of Fisheries Management*, *33*, 652–664.

Cabonce, J., Fernando, R., Wang, H., & Chanson, H. (2019). Using small triangular baffles to facilitate upstream fish passage in standard box culverts. *Environmental Fluid Mechanics*, *19*(1), 157–179. https://doi.org/10.1007/s10652-018-9604-x

Cabonce, J., Wang, H., & Chanson, H. (2018). Ventilated corner baffles to assist upstream passage of small-bodied fish in box culverts. *Journal of Irrigation and Drainage Engineering*, *144*(8), 0418020. https://doi.org/10.1061/(ASCE)IR.1943-4774.0001329

Cahoon, J. E., McMahon, T., Solcz, A., Blank, M., & Stein, O. (2007). *Fish passage in Montana culverts: Phase II - passage goals*. Report FHWA/MT-07-010/8181, Montana Department of Transportation and US Department of Transportation, Federal Highway Administration, 61 pages.

Chanson, H. (2019). Utilising the boundary layer to help restore the connectivity of fish habitats and populations. An engineering discussion. *Ecological Engineering*, *141*, 105613. https://doi.org/10.1016/j.ecoleng.2019.105613

Chanson, H. (2020). Low velocity zone in smooth pipe culvert with and without streamwise rib for fish passage. *Journal of Hydraulic Engineering*, *146*(9), 04020059. https://doi.org/10.1061/(ASCE)HY.1943-7900.0001789

Chanson, H., & Leng, X. (2021). *Fish swimming in turbulent waters. Hydraulics guidelines to assist upstream fish passage in box culverts*. Leiden, The Netherlands, 202 pages and 19 video movies: CRC Press, Taylor and Francis Group. https://doi.org/10.1201/9781003029694

Chin, D. A. (2013). Hydraulic analysis and design of pipe culverts: USGS versus FHWA. *Journal of Hydraulic Engineering, ASCE*, *139*(8), 886–893.

Dodd, C. K., Jr., Barichivich, W. J., & Smith, L. L. (2004). Effectiveness of a barrier wall and culverts in reducing wildlife mortality on a heavily traveled highway in Florida. *Biological Conservation*, *118*, 619–631.

Doehring, K., Young, R. G., & McIntosh, A. R. (2011). Factors affecting juvenile galaxiid fish passage at culverts. *Marine and Freshwater Research*, *62*, 38–45.

Feurich, R., Boubee, J., & Olsen, N. R. B. (2012). Improvement of fish passage in culverts using CFD. *Ecological Engineering*, *47*, 1–8.

Garner, M. E. (2011). *Model study of the hydraulics related to fish passage through embedded culverts*. (Master's thesis), University of Sakatchewan, Canada, 263 pages.

Gerard, R. (1978). Secondary flow in noncircular conduits. *Journal of Hydraulic Division, ASCE*, *104*(HY5), 755–773.

Gessner, F. B. (1973). The origin of secondary flow in turbulent flow along a corner. *Journal of Fluid Mechanics*, *58*, Part 1, 1–25.

Gigleux, M., & de Billy, V. (2013). "Petits ouvrages hydrauliques et continuités écologiques. Cas de la faune piscicole." *Note d'Information - Économie Environnement Conception - Série(EEC) No. 96*, Service d'études sur les transports, les routes et leurs aménagements, Provins, France, 25 pages (in French).

Goerig, E., Bergeron, N. E., & Castro-Santos, T. (2017). Swimming behaviour and ascent paths of brook trout in a corrugated culvert. *River Research and Applications*, *33*, 1463–1471.

Goettel, M. T., Atkinson, J. F., & Bennett, S. J. (2015). Behavior of western blacknose dace in a turbulence modified flow field. *Ecological Engineering*, *74*, 230–240.

Goosem, M. (2002). Effects of tropical rainforest roads on small mammals: Fragmentation, edge effects and traffic disturbance. *Wildlife Research*, *29*, 277–289.

Goring, D. G., & Nikora, V. I. (2002). Despiking acoustic doppler velocimeter data. *Journal of Hydraulic Engineering*, *128*(1), 117–126 Discussion: Vol. 129, No. 6, pp. 484–489.

Henderson, F. M. (1966). *Open channel flow*. New York, USA: MacMillan Company.

Humphries, P., & Walker, K. (2013). *Ecology of Australian freshwater fishes*. Clayton, Australia: CSIRO Publishing 436 pages.

Hurst, T. P., Kay, B. H., Ryan, P. A., & Brown, M. D. (2007). Sublethal effects of mosquito larvicides on swimming performances of larvivorous fish *Melanotaenia duboulayi* (Atheriniformes: Melanotaeniidae). *Journal of Economic Entomololy*, *100*(1), 61–65.

Imamoto, H., & Ishigaki, T. (1986). *Visualization of longitudinal eddies in an open channel flow*. Proceedings of 4th International Symposium on Flow Visualization, 26–29 August, Paris, France, pp. 333–337.

Januchowski-Hartley, S. R., Diebel, M., Doran, P. J., & McIntyre, P. B. (2014). Predicting road culvert passability for migratory fishes. *Diversity and Distributions*, *20*, 1414–1424.

Jensen, K. M. (2014). Velocity reduction factors in near boundary flow and the effect on fish passage through culverts. (Master of Science thesis). Brigham Young University, USA, 44 pages.

Jones, M. J., & Hale, R. (2020). Using knowledge of behaviour and optic physiology to improve fish passage through culverts. *Fish and Fisheries*, *00*, 1–13. https://doi.org/10.1111/faf.12446

Katopodis, C., & Gervais, R. (2016). "Fish swimming performance database and analyses." DFO CSAS Research Document No. 2016/002, Canadian Science Advisory Secretariat, Fisheries and Oceans Canada, Ottawa, Canada, 550 pages.

Kemp, P. (2012). Bridging the gap between fish behaviour, performance and hydrodynamics: An ecohydraulics approach to fish passage research. *River Research and Applications*, *28*, 403–406. https://doi.org/10.1002/rra.1599

Kern, P., Cramp, R., Gordos, M. A., Watson, J., & Franklin, C. (2018). Measuring U_{crit} and endurance: Equipment choice influences estimates of fish swimming performance. *Journal of Fish Biology*, *92*, 237–247.

Khodier, M. A., & Tullis, B. P. (2014). Fish passage behavior for severe hydraulic conditions in baffled culverts. *Journal of Hydraulic Engineering, ASCE*, *140*(3), 322–327. https://doi.org/10.1061/(ASCE)HY.1943-7900.0000831

Khodier, M. A., & Tullis, B. P. (2018). Experimental and computational comparison of baffled-culvert hydrodynamics for fish passage. *Journal of Applied Water Engineering and Research*, *6*(3), 191–199. https://doi.org/10.1080/23249676.2017.1287018

Larinier, M. (2002). Fish passage through culverts, rock weirs and estuarine obstructions. *Bulletin Français de Pêche et Pisciculture*, *364*-(Supplement), 119–134.

Leng, X., Chanson, H., Gordos, M., & Riches, M. (2021). Novel Hydraulics guidelines can assist upstream fish passage through smooth box culverts. *Australasian Journal of Water Resources*, 1–10. https://doi.org/10.1080/13241583.2020.1792091

Liggett, J. A., Chiu, C. L., & Miao, L. S. (1965). Secondary currents in a corner. *Journal of Hydraulic Division*, *91*(HY6), 99–117.

Macdonald, J. I., & Davies, O. E. (2007). Improving the upstream passage of two galaxiid fish species through a pipe culvert. *Fisheries Management and Ecology*, *14*, 221–230.

Monk, S. K., & Hotchkiss, R. H. (2012). Culvert roughness elements for native Utah fish passage: Phase II. Report no. UT-12.09. Utah Department of Transportation - Research Division, USA, 47 pages.

Montes, J. S. (1997). Transition to a free-surface flow at end of a horizontal conduit. *Journal of Hydraulic Research*, *35*(2), 225–241.

Montes, J. S. (1998). *Hydraulics of open channel flow* (p. 697). New-York, NY: ASCE Press.

Naot, D., & Rodi, W. (1982). Calculation of secondary currents in channel flow. *Journal of Hydraulic Division*, *108*(HY8), 948–967.

Nezu, I., & Nakagawa, H. (1993). Turbulence in open-channel flows. *IAHR Monograph*, IAHR fluid mechanics section, Balkema Publ., Rotterdam, The Netherlands, 281 pages.

Nezu, I., & Rodi, W. (1985). Experimental study on secondary currents in open channel flow. *Proceedings 21st IAHR Biennial Congress*, Melbourne, Australia, pp. 114–119.

Olsen, A., & Tullis, B. (2013). Laboratory study of fish passage and discharge capacity in slip-lined, baffled culverts. *Journal of Hydraulic Engineering, ASCE*, *139*(4), 424–432.

Papanicolaou, A. N., & Talebbeydokhti, N. (2002). Discussion of "turbulent open-channel flow in circular corrugated culverts.". *Journal of Hydraulic Engineering*, *128*(5), 548–549.

Pavlov, D. S., Lupandin, A. I., & Skorobogatov, M. A. (1994). Influence of flow turbulence on critical flow velocity for Gudgeon (*Gobio gobio*). *Doklady Biological Sciences*, *336*, 215–217 Translated from *DokladyAkademii Nauk*, ∼l. 336, No. 1, 1994, pp. 138–141.

Pavlov, D. S., Skorobogatov, M. A., & Shtaf, L. G. (1982). Influence of stream turbulence on the magnitude of the critical current velocity for fish. *Doklady Biological Sciences*, *267*, 560–562 Translated from *DokladyAkademii Nauk*, ∼l. 267, No. 4, 1982, pp. 1019–1021.

Pearson, W., Richmond, M., Johnson, G., Sargeant, S., Mueller, R., Cullinan, V., Deng, Z., Dibrani, B., Guensch, G., May, C., O'rourke, L., Sobocinski, K., and Tritico, H. (2005). "Protocols for evaluation of upstream passage of juvenile salmonids in an experimental culvert test bed." Report No. PNWD-3525, Washington State Department of Transportation, USA, 93 pages.

Perkins, H. J. (1970). The formation of streamwise vorticity in turbulent flow. *Journal of Fluid Mechanics*, *44*, Part 4, 721–740.

Prandtl, L. (1926). "*Turbulent flow*." International Congress for Applied Mechanics, Zurich, Switzerland, 21 pages. (Also Technical Memorandum NACA No. 435, 1927).

Prandtl, L. (1952). *Essentials of fluid dynamics with applications to hydraulics, aeronautics, meteorology and other subjects*. London, UK: Blackie & Son 452 pages.

Rajaratnam, N., & Katopodis, C. (1990). Hydraulics of culvert fishways III: Weir baffle culvert fishways. *Canadian Journal of Civil Engineering, Vo.*, *17*, 558–568.

Rogers, K. M., Rummel, S. M., Lavelle, K. M., Duchamp, J. E., Niles, J. M., & Janetski, D. J. (2021). A comparison of brook trout passage at road culverts to Broadscale Assessment Criteria in a Pennsylvania headwater stream. *North American Journal of Fisheries Management*, 8 pages, *41*, 1351–1359. https://doi.org/10.1002/nafm.10648

Sanchez, P. A., Leng, X., Von Brandis-Martini, J., & Chanson, H. (2020). Hybrid modelling of low velocity zones in an asymmetrical channel with sidewall longitudinal rib to assist fish passage. *River Research and Applications*, *36*(5), 807–818. https://doi.org/10.1002/rra.3600

Santos, H. A., Dupont, E., Aracena, F., Dvorak, J., Pinheiro, A., Teotonio, M., & Paula, A. (2021). Stairs pipe culverts: Flow simulations and implications for the passage of European and Neotropical fishes. *Journal of Ecohydraulics*, *6*(1), 36–52. https://doi.org/10.1080/24705357.2020.1713918

Shaft, L. G., Pavlov, D. S., Skorobogatov, M. A., and Barekyan, A. S. (1983). *Voor. Ikhtiol.*, *23*, 2, pp. 307–317 (in Russian).

Skorobogatov, M. A., & Pavlov, S. D. (1991). A study of the orientation of young roach, *Rutilus rutilus*, with respect to current velocity. *Voprosy Ikhtiologii*, *31*(3), 516–520.

British Standard. (1943). *"Flow measurement." British Standard Code BS 1042:1943*. London: British Standard Institution.

Sterling, M. (1998). *A study of boundary shear stress, flow resistance and the free overfall in open channels with a circular cross section*. (PhD thesis), University of Birmingham, School of Civil Engineering, Birmingham, U.K., 541 pages.

Tamburrino, A., & Gulliver, J. S. (2007). Free-surface visualization of streamwise vortices in a channel flow. *Water Resources Research*, *43*, W11410, 12 pages. https://doi.org/10.1029/2007WR005988

Tominaga, A., Nezu, I., Ezaki, K., & Nakagawa, H. (1989). Three-dimensional turbulent structure in straight open channel flows. *Journal of Hydraulic Research*, *27*(1), 149–173.

Tonkin, J. D., Wright, L. A. H., & David, B. O. (2012). Mussel spat ropes assist redfin bully Gobiomorphus huttoni passage through experimental culverts with velocity barriers. *Water*, *4*, 683–689.

Tudorache, C., Viaene, P., Blust, R., Vereecken, H., & De Boeck, G. (2008). A comparison of swimming capacity and energy use in seven European freshwater fish species. *Ecology of Freshwater Fish*, *17*, 284–291.

Wahl, T. L. (2003). Despiking acoustic doppler velocimeter data. *Journal of Hydraulic Engineering, ASCE*, *129*(6), 484–487.

Wang, H., & Chanson, H. (2018). Modelling upstream fish passage in standard box culverts: Interplay between turbulence, fish kinematics, and energetics. *River Research and Applications*, *34*(3), 244–252. https://doi.org/10.1002/rra.3245

Wang, H., Chanson, H., Kern, P., & Franklin, C. (2016). *Culvert hydrodynamics to enhance upstream fish passage: Fish response to turbulence*. Ivey, G., Zhou, T., Jones, N., & Draper, S. (Eds.). Proceedings of 20th Australasian Fluid Mechanics Conference, Australasian Fluid Mechanics Society, Perth WA, Australia, 5–8 December, Paper 682, 4 pages.

Warren, M. L., Jr., & Pardew, M. G. (1998). Road crossings as barriers to small-stream fish movement. *Transactions of the American Fisheries Society*, *127*, 637–644.

Williams, J. G., Armstrong, G., Katopodis, C., Larinier, N., & Travade, F. (2012). Thinking like a fish: A key ingredient for development of effective fish passage facilities at river obstructions. *River Research and Applications*, *28*, 407–417.

SUPPORTING INFORMATION

Additional supporting information may be found in the online version of the article at the publisher's website.

How to cite this article: Li, Z., Harley, J., & Chanson, H. (2022). Physical modelling of pipe culverts to assist upstream fish passage. *River Research and Applications*, *38*(2), 309–322. https://doi.org/10.1002/rra.3905